Contribution from the Department of Chemistry,
Tulane University, New Orleans, Louisiana 70118

Ligand Substitution Processes in Tetranuclear Carbonyl Clusters. 4. Molecular Structure and Reactivity of $Ir_4(CO)_8[P(CH_3)_3]_4$

DONALD J. DARENSBOURG* and BRENDA J. BALDWIN-ZUSCHKE

Received February 25, 1981

The structure of $Ir_4(CO)_8[PMe_3]_4$ has been determined by a single-crystal X-ray investigation. The structure consists of a slightly distorted tetrahedron of iridium atoms containing three symmetrical edge-bridging CO ligands along one triangular face and each metal atom bearing a trimethylphosphine ligand. The geometry of phosphines about the tetranuclear metal centers is one apical, two axial, and one equatorial. The complex crystallizes in the monoclinic space group $P2_1/n$ with a = 12.114 (4) Å, b = 12.469 (5) Å, c = 22.056 (5) Å, β = 98.91 (2)°, V = 3291 (2) Å^3, Z = 4, and ρ(calcd) = 2.62 g cm^{-3}. Diffraction data (2θ out to 55°) were collected with a four-circle autodiffractometer using Mo K$\bar{\alpha}$ radiation. The structure was refined by using the full-matrix least-squares procedure, and the resulting discrepancy indices were R_1 = 0.058 and R_2 = 0.074 for 5043 independent reflections. Important bond distance parameters are as follows: Ir–Ir (apical–basal) = 2.737 (1,2,2,3) Å, Ir–Ir (basal–basal) = 2.720 (1,5,5,2) Å and 2.794 (1) Å (where the longer bond involves the iridium atoms with axial PMe_3 ligands), and Ir–P = 2.312 (6,14,23,4) Å.[1] The reaction of $Ir_4(CO)_8[PMe_3]_4$ with CO to afford $Ir_4(CO)_9[PMe_3]_3$ was found to occur via a dissociative process and at a rate 3300 times slower than that for the analogous process involving the sterically more demanding PEt_3 ligand.

Introduction

Kinetic parameters for carbon monoxide substitutional processes in tetranuclear iridium carbonyl cluster species have revealed substantial rate enhancement for *dissociative* carbon monoxide loss with progressive substitution of triphenylphosphine in the cluster's coordination sphere.[2] In view of the spatial requirements of the triphenylphosphine ligand (ligand cone angle = 145°),[3] it is anticipated that this behavior is at least in part due to steric effects. Indeed, sizable steric acceleration of ligand dissociation processes in mononuclear metal carbonyl phosphine and phosphite derivatives is well documented.[4] Current efforts in our laboratories to assess steric effects on ligand substitutional processes in metal carbonyl clusters involve the evaluation of kinetic data for carbon monoxide exchange in $M_4(CO)_{12-n}L_n$ derivatives, where M = Co, Rh, and Ir (eq 1).[5-7]

$$M_4(CO)_{12-n}L_n + {}^{13}CO \rightleftharpoons M_4(CO)_{12-n-m}({}^{13}CO)_mL_n + CO \quad (1)$$

In the cases where steric crowding in the metal cluster is severe, i.e., n = 4, phosphine dissociation becomes an important consideration (eq 2). In order to judiciously determine the

$$M_4(CO)_8L_4 + CO \rightarrow M_4(CO)_9L_3 + L \quad (2)$$

role of steric contributions to these substitutional processes, it is imperative to know the stereochemical arrangement of the phosphorus donor ligands about the metal tetrahedron. Hence, one member of this class, $Ir_4(CO)_8[PMe_3]_4$, has been fully characterized via single-crystal X-ray diffraction studies and is reported upon herein. In addition, comparative investigations of solution geometry and reactivity toward phosphine loss of this derivative with other $Ir_4(CO)_8[PR_3]_4$ are presented.

Experimental Section

Synthesis of $Ir_4(CO)_8[PMe_3]_4$. $Ir_4(CO)_{12}$ (0.37 g, 0.70 mmol) and toluene (70 mL) were combined in a round-bottom flask fitted with a Dewar condenser which was cooled with a dry ice/acetone slush.[8] The reaction system was placed under a carbon monoxide atmosphere, and 0.70 mL of PMe_3 was syringed in. After a 2-h reflux, all solvent was removed by vacuum, and 10 mL of ethanol was added to the resultant oil. The bright orange crystals were filtered, washed with 2 mL of cold ethanol, and dried in vacuo. Recrystallization from hot ethanol afforded crystals of $Ir_4(CO)_8[PMe_3]_4$ suitable for X-ray analysis. Anal. Calcd for $Ir_4(CO)_8[P(CH_3)_3]_4$: C, 18.51; H, 2.78. Found: C, 18.26; H, 2.81.

Reaction of $Ir_4(CO)_8[PMe_3]_4$ with CO. The reaction of $Ir_4(CO)_8[PMe_3]_4$ with CO to afford $Ir_4(CO)_9[PMe_3]_3$ was carried out in a Schlenk flask in tetrachloroethylene solvent under a static atmosphere of carbon monoxide. The flask was fitted with a septum cap secured by copper wire and was placed in a constant-temperature bath. Samples were withdrawn at regular time intervals with a hypodermic syringe for infrared spectral analysis. Infrared spectra were recorded on a Perkin-Elmer 283B spectrophotometer using matched sodium chloride cells (1.0 mm).

Crystallographic Studies. Crystallographic analyses were carried out by Dr. Cynthia S. Day at Crystalytics Co., Lincoln, Nebraska. An irregular-shaped red crystal of $Ir_4(CO)_8[P(CH_3)_3]_4$, with minimum and maximum dimensions of 0.35 and 0.55 mm, respectively, was glued to the end of a thin glass fiber having a tip diameter of 0.20 mm with the long dimension of the crystal nearly parallel to the ϕ axis of the diffractometer in order to minimize absorption effects. This crystal was then accurately centered optically on a computer-controlled four-circle Nicolet autodiffractometer, and a total of 15 high-angle ($2\theta_{MoK\bar{\alpha}} < 20°$) reflections were used to align the crystal and calculate angular settings for each reflection. A least-squares refinement of the diffraction geometry for these 15 reflections recorded at ambient laboratory temperature of 20 ± 1 °C with graphite-monochromated Mo K$\bar{\alpha}$ radiation (λ = 0.710 73 Å) showed the crystal to belong to the monoclinic system with lattice constants a = 12.114 (4) Å, b = 12.469 (5) Å, c = 22.056 (5) Å, and β = 98.91 (2)°. Systematic absences indicated the space group to be $P2_1/n$ (a special setting of $P2_1/n$—C_{2h}^5 (No. 14)).[9] A unit cell of four $Ir_4(CO)_8[P(CH_3)_3]_4$ molecules per 3291 (2) Å^3 afforded a calculated density of 2.62 g cm^{-3}. The linear absorption coefficient of the crystal for Mo K$\bar{\alpha}$ radiation is 173.3 cm^{-1}.[10a]

Intensity measurements utilized graphite-monochromated Mo K$\bar{\alpha}$ radiation and the ω scanning technique with a 4° takeoff angle and

(1) The first number in parentheses following the averaged value of a bond length is the root-mean-square estimated standard deviation of an individual datum. The second and third numbers, when given, are the average and maximum deviations from the averaged value, respectively. The fourth number represents the number of individual measurements which are included in the average value.
(2) Karel, K. J.; Norton, J. R. *J. Am. Chem. Soc.* **1974**, *96*, 6812.
(3) Tolman, C. A. *Chem. Rev.* **1977**, *77*, 313.
(4) Darensbourg, D. J.; Graves, A. H. *Inorg. Chem.* **1979**, *18*, 1257.
(5) Darensbourg, D. J.; Incorvia, M. J. *J. Organomet. Chem.* **1979**, *171*, 89.
(6) Darensbourg, D. J.; Incorvia, M. J. *Inorg. Chem.* **1980**, *19*, 2585.
(7) Darensbourg, D. J.; Incorvia, M. J. *Inorg. Chem.* **1981**, *20*, 1911.
(8) Drakesmith, A. J.; Whyman, R. *J. Chem. Soc., Dalton Trans.* **1973**, 362.
(9) "International Tables for X-Ray Crystallography"; Kynoch Press: Birmingham, England, 1969; Vol. I.
(10) "International Tables for X-Ray Crystallography"; Kynoch Press: Birmingham, England, 1974; Vol. IV: (a) pp 55-66; (b) pp 149-150.

0020-1669/81/1320-3846$01.25/0

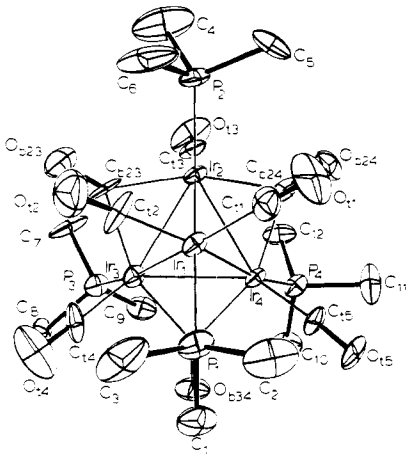

Figure 1. Perspective ORTEP drawing of $Ir_4(CO)_8[P(CH_3)_3]_4$. Nonhydrogen atoms are represented by thermal vibration ellipsoids drawn to encompass 50% of the electron density.

a normal-focus X-ray tube. A total of 7563 independent reflections having $2\theta \leq 55°$ were measured in three concentric shells of increasing 2θ. A scanning rate of 4°/min was employed for the scan between ω settings 0.45° respectively above and below the calculated K$\bar{\alpha}$ doublet value for those reflections having $3° < 2\theta_{MoK\bar{\alpha}} \leq 43.0°$, and a scanning rate of 3°/min was used for reflections having $43° < 2\theta_{MoK\bar{\alpha}} \leq 55°$. Each of these 0.90° scans was divided into 19 equal time intervals, and those 13 contiguous intervals which had the highest single accumulated count at their midpoint were used to calculate the net intensity from scanning. Background counts, each lasting for one-fourth the total time used for the net scan, were measured at settings 0.9° above and below the calculated value for each reflection. The six standard reflections, measured every 300 reflections as a monitor for possible disalignment and/or deterioration of the crystal, gave no indication of either. The intensity data were corrected empirically for absorption effects with the use of ψ scans for three reflections having 2θ values between 13 and 17° and were then reduced to relative squared amplitudes, $|F_o|^2$, by means of standard Lorentz and polarization corrections.

Of the 7563 reflections examined, 2520 were eventually rejected as unobserved by applying the rejection criterion $I < 3.0\sigma(I)$, where $\sigma(I)$ is the standard deviation in the intensity computed from $\sigma^2(I) = (C_t + k^2B)$ where C_t is the total scan count, k is the ratio of scan time to background time, and B is the total background count.

The four iridium atoms were located with the use of direct methods; the 32 remaining nonhydrogen atoms appeared in a single difference Fourier synthesis based on refined parameters for the iridium atoms [$R_1 = 0.168$ for 2900 independent reflections having $2\theta_{MoK\bar{\alpha}} < 43°$ and $I > 3\sigma(I)$]. Isotropic unit-weighted full-matrix least-squares refinement for the 36 nonhydrogen atoms gave R_1 (unweighted, based

$$R_1 = \sum||F_o| - |F_c||/\sum|F_o| \qquad R_2 = [\sum w(|F_o| - |F_c|)^2\sum|F_o|^2]^{1/2}$$

on F) = 0.092 and R_2 (weighted) = 0.100 where anisotropic refinement converged to $R_1 = 0.049$ and $R_2 = 0.053$ for 2900 reflections having $2\theta_{MoK\bar{\alpha}} < 43°$ and $I > 3\sigma(I)$.[11] These and all subsequent structure factor calculations employed the atomic form factors compiled by Cromer and Mann[12] and an anomalous dispersion correction to the scattering factors of the iridium and phosphorus atoms.[10b]

The final cycles of empirically weighted[13,14] full-matrix least-squares refinement, in which the structural parameters for all nonhydrogen atoms were varied, converged to $R_1 = 0.058$, $R_2 = 0.074$, and GOF = 1.29[15] for 5043 independent reflections having $2\theta_{MoK\bar{\alpha}} \leq 55.0°$ and $I > 3\sigma(I)$. During the final cycle of refinement, no parameter shifted by more than $0.13\sigma_p$ with the average shift being less than $0.01\sigma_p$ where σ_p is the estimated standard deviation of the parameter. The only peaks in the final difference Fourier significantly above the noise level were within 1.5 Å of the Ir atoms.

All calculations were performed on a Data General Eclipse S-200 computer with 64 K of 16-bit words, a parallel floating-point processor for 32- and 64-bit arithmetic, and a Data General disk with 10 million 16-bit words using versions of the Nicolet (Syntex) E-XTL or SHELXTL

Table I. Atomic Coordinates for Nonhydrogen Atoms in Crystalline $Ir_4(CO)_8(P(CH_3)_3)_4$[a]

atom type[b]	fractional coordinates		
	10^4x	10^4y	10^4z
Ir_1	2987.8 (6)	1710.5 (5)	4195.6 (4)
Ir_2	3043.0 (6)	3150.6 (5)	3263.3 (3)
Ir_3	2626.5 (6)	3845.1 (6)	4372.6 (3)
Ir_4	1051.3 (6)	2617.7 (5)	3611.7 (3)
P_1	2339 (5)	965 (5)	5045 (3)
P_2	4465 (5)	2425 (5)	2824 (3)
P_3	2345 (5)	5683 (4)	4339 (3)
P_4	−384 (4)	3482 (4)	2992 (3)
O_{t1}	2860 (22)	−305 (15)	3428 (11)
O_{t2}	5371 (18)	1787 (21)	4847 (11)
O_{t3}	2761 (18)	5024 (15)	2389 (11)
O_{t4}	3467 (25)	3755 (16)	5726 (10)
O_{t5}	−430 (16)	790 (14)	3813 (9)
O_{b23}	4991 (15)	4260 (15)	4089 (10)
O_{b24}	1499 (16)	1705 (15)	2379 (8)
O_{b34}	268 (14)	3780 (15)	4693 (8)
C_{t1}	2899 (19)	455 (21)	3707 (11)
C_{t2}	4476 (16)	1798 (18)	4589 (13)
C_{t3}	2875 (18)	4285 (21)	2724 (11)
C_{t4}	3112 (22)	3825 (17)	5205 (10)
C_{t5}	168 (18)	1486 (16)	3725 (10)
C_{b23}	4081 (13)	3945 (17)	3974 (11)
C_{b24}	1755 (13)	2194 (13)	2820 (11)
C_{b34}	941 (15)	3555 (14)	4408 (9)
C_1	1208 (27)	1544 (20)	5389 (14)
C_2	1841 (29)	−415 (19)	4920 (17)
C_3	3420 (27)	825 (32)	5712 (17)
C_4	5197 (37)	3407 (36)	2402 (23)
C_5	4017 (36)	1360 (41)	2251 (21)
C_6	5608 (29)	1827 (41)	3349 (16)
C_7	3290 (21)	6451 (22)	3967 (16)
C_8	2495 (21)	6304 (21)	5092 (13)
C_9	966 (21)	6154 (21)	3983 (11)
C_{10}	−1399 (22)	4209 (25)	3348 (13)
C_{11}	−1303 (24)	2547 (22)	2513 (15)
C_{12}	19 (23)	4436 (22)	2434 (11)

[a] The numbers in parentheses are the estimated standard deviations in the last significant digit. [b] Atoms are labeled in agreement with Figure 1.

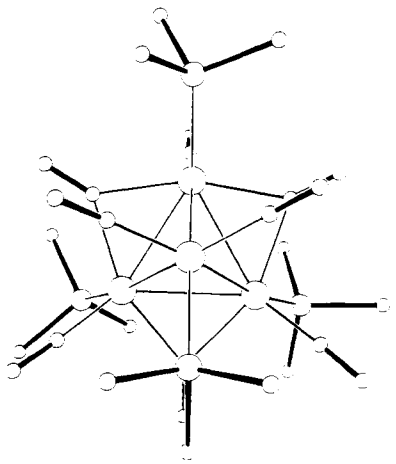

Figure 2. Projection of the molecule $Ir_4(CO)_8[P(CH_3)_3]_4$ on the basal Ir_3 plane to more clearly describe the stereochemistry of CO and PMe_3 ligands around the Ir_4 unit.

(11) The anisotropic thermal parameter is of the form $\exp[-0.25(B_{11}h^2a^{*2} + B_{22}k^2b^{*2} + B_{33}l^2c^{*2} + 2B_{12}hka^*b^* + 2B_{13}hla^*c^* + 2B_{23}klb^*c^*)]$.
(12) Cromer, D. T.; Mann, J. L. *Acta Crystallogr., Sect. A* **1968**, *A24*, 321.
(13) The weighting scheme used in the least-squares minimization of the function $\sum w(|F_o| - |F_c|)^2$ is defined as $w = 1/\sigma_F^2$.
(14) For empirical weights, $\sigma_F = \sum_0^3 a_n|F_o|^n = a_0 + a_1|F_o| + a_2|F_o|^2 + a_3|F_o|^3$, with the a_n being coefficients from the least-squares fitting of the curve $||F_o| - |F_c|| = \sum_0^3 a_n|F_o|^n$. In this case, $a_0 = 5.58$, $a_1 = 1.51 \times 10^{-2}$, $a_2 = 2.62 \times 10^{-5}$, and $a_3 = -2.82 \times 10^{-8}$.
(15) GOF = $[\sum w(|F_o| - |F_c|)^2/(NO - NV)]^{1/2}$ where NO is the number of observations and NV is the number of variables.

Table II. Anisotropic Thermal Parameters for Nonhydrogen Atoms in Crystalline $Ir_4(CO)_8(P(CH_3)_3)_4$[a,b]

atom type[c]	B_{11}	B_{22}	B_{33}	B_{12}	B_{13}	B_{23}
Ir_1	1.72 (2)	1.20 (2)	3.08 (3)	0.05 (2)	0.61 (2)	0.38 (2)
Ir_2	1.55 (2)	1.27 (2)	2.97 (3)	−0.02 (2)	1.04 (2)	0.27 (2)
Ir_3	1.99 (3)	1.32 (2)	2.80 (3)	−0.17 (2)	0.60 (2)	−0.09 (2)
Ir_4	1.29 (2)	1.36 (2)	2.65 (3)	−0.14 (2)	0.63 (2)	0.16 (2)
P_1	3.6 (3)	2.3 (2)	4.1 (3)	0.1 (2)	1.5 (2)	1.1 (2)
P_2	2.3 (2)	2.5 (2)	4.3 (3)	0.4 (2)	2.0 (2)	−0.0 (2)
P_3	3.0 (2)	1.3 (2)	3.5 (2)	−0.1 (2)	1.2 (2)	−0.2 (2)
P_4	1.7 (2)	1.9 (2)	3.4 (2)	0.3 (2)	0.4 (2)	0.4 (2)
O_{t1}	9.0 (15)	2.6 (8)	8.2 (14)	1.7 (9)	0.7 (12)	−3.1 (9)
O_{t2}	4.5 (10)	7.6 (14)	5.9 (12)	−0.1 (10)	−1.1 (8)	−0.8 (10)
O_{t3}	5.4 (10)	3.5 (9)	8.7 (14)	−0.3 (8)	2.3 (10)	4.0 (9)
O_{t4}	11.8 (19)	3.3 (9)	4.5 (10)	2.5 (11)	−1.3 (11)	−0.5 (7)
O_{t5}	5.1 (9)	3.3 (8)	5.4 (9)	−3.4 (7)	1.4 (7)	0.2 (7)
O_{b23}	3.1 (7)	3.7 (8)	7.1 (11)	−0.5 (7)	1.8 (7)	−1.1 (8)
O_{b24}	4.7 (9)	4.0 (8)	4.2 (8)	0.0 (7)	0.8 (7)	−2.3 (7)
O_{b34}	3.1 (7)	4.9 (9)	4.1 (8)	1.5 (7)	1.9 (6)	0.0 (7)
C_{t1}	2.4 (8)	4.3 (11)	3.5 (10)	0.2 (8)	−0.6 (7)	−0.3 (9)
C_{t2}	1.2 (7)	2.5 (9)	7.2 (15)	−0.6 (7)	−0.7 (8)	1.3 (9)
C_{t3}	2.2 (8)	4.2 (11)	4.2 (11)	−0.9 (8)	1.9 (8)	−0.2 (9)
C_{t4}	5.3 (12)	1.7 (8)	2.6 (9)	−1.4 (8)	−1.7 (8)	0.3 (7)
C_{t5}	2.7 (8)	1.7 (7)	3.7 (9)	−1.3 (6)	0.50 (7)	0.5 (7)
C_{b23}	1.0 (5)	3.1 (9)	6.1 (12)	0.0 (5)	2.0 (7)	1.1 (8)
C_{b24}	1.3 (5)	0.8 (6)	6.3 (12)	0.8 (5)	1.5 (6)	−0.1 (7)
C_{b34}	1.8 (7)	1.0 (6)	3.5 (8)	−0.2 (5)	1.5 (6)	−1.0 (6)
C_1	6.5 (16)	2.5 (10)	5.4 (14)	−0.9 (10)	3.1 (12)	0.4 (9)
C_2	7.4 (18)	1.4 (8)	8.9 (20)	1.7 (10)	4.4 (16)	1.5 (11)
C_3	4.7 (15)	8.5 (23)	7.1 (19)	−1.0 (15)	0.6 (13)	5.6 (18)
C_4	8.4 (25)	7.7 (24)	11.9 (32)	2.5 (20)	6.5 (24)	5.3 (23)
C_5	8.5 (25)	12.6 (35)	10.4 (28)	−2.1 (23)	5.5 (23)	−9.4 (28)
C_6	5.3 (17)	13.4 (34)	5.9 (17)	2.5 (20)	4.1 (14)	4.3 (20)
C_7	2.9 (10)	3.5 (11)	9.1 (20)	−0.1 (9)	4.0 (12)	1.4 (12)
C_8	3.0 (10)	3.7 (11)	5.7 (14)	−0.2 (9)	0.1 (9)	−3.2 (10)
C_9	3.7 (11)	3.5 (11)	4.1 (11)	1.5 (9)	1.3 (9)	−0.2 (9)
C_{10}	3.3 (11)	5.4 (15)	4.7 (13)	1.3 (11)	0.8 (9)	0.7 (11)
C_{11}	4.1 (12)	3.3 (11)	6.7 (16)	0.2 (10)	−1.7 (11)	−1.9 (11)
C_{12}	4.3 (11)	4.4 (12)	3.4 (10)	0.7 (10)	1.9 (9)	1.5 (9)

[a] The numbers in parentheses are the estimated standard deviations in the last significant digit. [b] The form of the anisotropic thermal parameter is given in ref 11. [c] Atoms are labeled in agreement with Figure 1.

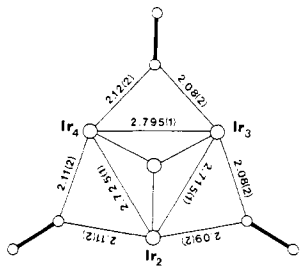

Figure 3. Iridium–carbon$_b$ and iridium–iridium bond distances in the basal Ir_3 plane.

interactive crystallographic software package as modified at Crystalytics Co.

Results and Discussion

The final atomic coordinates and anisotropic thermal parameters for all nonhydrogen atoms in $Ir_4(CO)_8[PMe_3]_4$ are provided in Tables I and II, respectively. The atomic numbering and thermal ellipsoids of the $Ir_4(CO)_8[PMe_3]_4$ molecule are shown in Figure 1. In Tables III and IV are given the individual bond distances and angles for all nonhydrogen atoms.

The four iridium atoms define a tetrahedron which is bridged on three edges by CO groups with a trimethylphosphine ligand bound to each iridium atom. The stereochemistry of carbonyl and phosphine ligands around the iridium cluster can best be seen in Figure 2, where two of the phosphines occupy axial sites in the basal Ir_3 plane. The observed symmetrical nature of the CO bridging groups is as anticipated for the nearly electronically equivalent basal

Table III. Bond Lengths Involving Nonhydrogen Atoms in Crystalline $Ir_4(CO)_8(P(CH_3)_3)_4$[a]

type[b]	length, Å	type[b]	length, Å
Ir_1-Ir_2	2.738 (1)	Ir_2-Ir_3	2.715 (1)
Ir_1-Ir_3	2.735 (1)	Ir_2-Ir_4	2.725 (1)
Ir_1-Ir_4	2.739 (1)	Ir_3-Ir_4	2.794 (1)
Ir_1-P_1	2.335 (6)	Ir_3-P_3	2.316 (5)
Ir_2-P_2	2.290 (6)	Ir_4-P_4	2.305 (5)
Ir_1-C_{t1}	1.90 (3)	Ir_2-C_{b23}	2.10 (2)
Ir_1-C_{t2}	1.88 (2)	Ir_3-C_{b23}	2.09 (2)
Ir_2-C_{t3}	1.84 (3)	Ir_2-C_{b24}	2.08 (2)
Ir_3-C_{t4}	1.84 (2)	Ir_4-C_{b24}	2.13 (2)
Ir_4-C_{t5}	1.81 (2)	Ir_3-C_{b34}	2.09 (2)
		Ir_4-C_{b34}	2.13 (2)
P_1-C_1	1.82 (3)	P_3-C_7	1.79 (3)
P_1-C_2	1.83 (3)	P_3-C_8	1.82 (3)
P_1-C_3	1.82 (4)	P_3-C_9	1.83 (3)
P_2-C_4	1.85 (5)	P_4-C_{10}	1.80 (3)
P_2-C_5	1.86 (5)	P_4-C_{11}	1.83 (3)
P_2-C_6	1.82 (4)	P_4-C_{12}	1.83 (3)
O_{t1}-C_{t1}	1.13 (3)	O_{b23}-C_{b23}	1.16 (3)
O_{t2}-C_{t2}	1.14 (3)	O_{b24}-C_{b24}	1.15 (3)
O_{t3}-C_{t3}	1.18 (3)	O_{b34}-C_{b34}	1.14 (3)
O_{t4}-C_{t4}	1.17 (3)		
O_{t5}-C_{t5}	1.17 (3)		

[a] The numbers in parentheses are the estimated standard deviations in the last significant digit. [b] Atoms are labeled in agreement with Figure 1.

iridium atoms (see Figure 3). The apical–basal iridium–iridium bonding distances have little scatter, varying from 2.735 to 2.739 Å. Two of the basal–basal iridium–iridium bonds are quite similar with bonding distances of 2.715 and

Table IV. Bond Angles Involving Nonhydrogen Atoms in Crystalline $Ir_4(CO)_8(P(CH_3)_3)_4$[a]

type[b]	angle, deg	type[b]	angle, deg
$Ir_2Ir_1Ir_3$	59.48 (3)	$Ir_1Ir_3Ir_2$	60.32 (3)
$Ir_2Ir_1Ir_4$	59.67 (3)	$Ir_1Ir_3Ir_4$	59.39 (3)
$Ir_3Ir_1Ir_4$	61.38 (3)	$Ir_2Ir_3Ir_4$	59.27 (3)
$Ir_1Ir_2Ir_3$	60.20 (3)	$Ir_1Ir_4Ir_2$	60.15 (3)
$Ir_1Ir_2Ir_4$	60.18 (3)	$Ir_1Ir_4Ir_3$	59.24 (3)
$Ir_3Ir_2Ir_4$	61.80 (3)	$Ir_2Ir_4Ir_3$	58.92 (3)
$Ir_2Ir_1P_1$	156.1 (2)	$Ir_1Ir_3P_3$	169.8 (1)
$Ir_3Ir_1P_1$	101.1 (2)	$Ir_2Ir_3P_3$	109.5 (1)
$Ir_4Ir_1P_1$	99.9 (2)	$Ir_4Ir_3P_3$	116.1 (1)
$Ir_1Ir_2P_2$	99.6 (2)	$Ir_1Ir_4P_4$	169.7 (1)
$Ir_3Ir_2P_2$	139.9 (2)	$Ir_2Ir_4P_4$	109.7 (1)
$Ir_4Ir_2P_2$	141.3 (2)	$Ir_3Ir_4P_4$	118.8 (1)
$Ir_2Ir_1C_{t1}$	96.9 (7)	$Ir_4Ir_2C_{t3}$	110.9 (8)
$Ir_2Ir_1C_{t2}$	100.1 (8)	$P_2Ir_2C_{t3}$	92.6 (8)
$Ir_3Ir_1C_{t1}$	152.8 (7)	$Ir_1Ir_3C_{t4}$	95.5 (7)
$Ir_3Ir_1C_{t2}$	92.3 (8)	$Ir_2Ir_3C_{t4}$	145.0 (7)
$Ir_4Ir_1C_{t1}$	96.0 (7)	$Ir_4Ir_3C_{t4}$	132.5 (7)
$Ir_4Ir_1C_{t2}$	152.1 (8)	$P_3Ir_3C_{t4}$	93.9 (7)
$P_1Ir_1C_{t1}$	97.6 (8)	$Ir_1Ir_4C_{t5}$	95.4 (7)
$P_1Ir_1C_{t2}$	94.0 (8)	$Ir_2Ir_4C_{t5}$	142.8 (7)
$C_{t1}Ir_1C_{t2}$	106.1 (11)	$Ir_3Ir_4C_{t5}$	135.0 (7)
$Ir_1Ir_2C_{t3}$	167.6 (8)	$P_4Ir_4C_{t5}$	92.2 (7)
$Ir_3Ir_2C_{t3}$	108.7 (8)		
$Ir_1Ir_2C_{b23}$	80.3 (6)	$P_3Ir_3C_{b23}$	93.3 (6)
$Ir_1Ir_2C_{b24}$	82.7 (5)	$P_3Ir_3C_{b34}$	91.9 (5)
$Ir_3Ir_2C_{b23}$	49.5 (6)	$C_{t4}Ir_3C_{b23}$	105.1 (9)
$Ir_3Ir_2C_{b24}$	112.0 (5)	$C_{t4}Ir_3C_{b34}$	97.1 (9)
$Ir_4Ir_2C_{b23}$	111.0 (6)	$C_{b23}Ir_3C_{b34}$	156.8 (8)
$Ir_4Ir_2C_{b24}$	50.3 (5)	$Ir_1Ir_4C_{b24}$	82.0 (5)
$P_2Ir_2C_{b23}$	95.7 (6)	$Ir_1Ir_4C_{b34}$	89.9 (5)
$P_2Ir_2C_{b24}$	97.6 (6)	$Ir_2Ir_4C_{b24}$	49.0 (5)
$C_{t3}Ir_2C_{b23}$	96.5 (9)	$Ir_2Ir_4C_{b34}$	105.7 (5)
$C_{t3}Ir_2C_{b24}$	97.9 (9)	$Ir_3Ir_4C_{b24}$	107.8 (5)
$C_{b23}Ir_2C_{b24}$	159.9 (8)	$Ir_3Ir_4C_{b34}$	47.8 (5)
$Ir_1Ir_3C_{b23}$	80.5 (6)	$P_4Ir_4C_{b24}$	89.5 (5)
$Ir_1Ir_3C_{b34}$	90.9 (5)	$P_4Ir_4C_{b34}$	95.4 (5)
$Ir_2Ir_3C_{b23}$	49.7 (6)	$C_{t5}Ir_4C_{b24}$	103.9 (8)
$Ir_2Ir_3C_{b34}$	107.4 (5)	$C_{t5}Ir_4C_{b34}$	101.5 (8)
$Ir_4Ir_3C_{b23}$	108.7 (6)	$C_{b24}Ir_4C_{b34}$	153.9 (7)
$Ir_4Ir_3C_{b34}$	49.2 (5)		
$Ir_2C_{b23}Ir_3$	80.8 (8)	$Ir_3C_{b34}Ir_4$	83.0 (7)
$Ir_2C_{b24}Ir_4$	80.7 (7)		
$Ir_1P_1C_1$	123.2 (10)	$Ir_3P_3C_7$	116.3 (10)
$Ir_1P_1C_2$	113.4 (11)	$Ir_3P_3C_8$	113.6 (9)
$Ir_1P_1C_3$	113.4 (12)	$Ir_3P_3C_9$	116.8 (8)
$C_1P_1C_2$	100.6 (14)	$C_7P_3C_8$	102.2 (13)
$C_1P_1C_3$	101.3 (15)	$C_7P_3C_9$	103.8 (13)
$C_2P_1C_3$	102.2 (16)	$C_8P_3C_9$	102.2 (12)
$Ir_2P_2C_4$	113.7 (15)	$Ir_4P_4C_{10}$	118.6 (10)
$Ir_2P_2C_5$	114.3 (15)	$Ir_4P_4C_{11}$	112.3 (10)
$Ir_2P_2C_6$	116.2 (13)	$Ir_4P_4C_{12}$	116.6 (9)
$C_4P_2C_5$	104.2 (21)	$C_{10}P_4C_{11}$	100.2 (13)
$C_4P_2C_6$	102.4 (20)	$C_{10}P_4C_{12}$	103.7 (13)
$C_5P_2C_6$	104.7 (20)	$C_{11}P_4C_{12}$	103.2 (13)
$Ir_1C_{t1}O_{t1}$	178 (2)	$Ir_2C_{b23}O_{b23}$	140 (2)
$Ir_1C_{t2}O_{t2}$	175 (2)	$Ir_3C_{b23}O_{b23}$	140 (2)
$Ir_2C_{t3}O_{t3}$	179 (2)	$Ir_2C_{b24}O_{b24}$	142 (2)
$Ir_3C_{t4}O_{t4}$	175 (2)	$Ir_4C_{b24}O_{b24}$	138 (2)
$Ir_4C_{t5}O_{t5}$	177 (2)	$Ir_3C_{b34}O_{b34}$	140 (2)
		$Ir_4C_{b34}O_{b34}$	137 (2)

[a] The numbers in parentheses are the estimated standard deviations in the last significant digit. [b] Atoms are labeled in agreement with Figure 1.

2.725, whereas one of the basal–basal iridium–iridium bonds (between Ir(3)–Ir(4)) is significantly longer at 2.794 Å (Figure 3). This bond lengthening apparently arises from *interligand* repulsions. The individual esd's on the above mentioned Ir–Ir bond distances are 0.001 Å. Other evidence of interligand repulsions is seen in the deviation from planarity of the three bridging CO groups with respect to the Ir_3 unit where the CO

Table V. Deviations of Bridging Carbonyls from Plane Defined by Ir_2, Ir_3, and Ir_4[a]

atom	dev from plane, Å
O_{b23}	−0.3321
O_{b24}	−0.1398
O_{b34}	0.6648
C_{b23}	−0.1838
C_{b24}	−0.0960
C_{b34}	0.3777

[a] Defined by $-0.3471X + 0.8354Y - 0.4262Z = 0.6408$, where X, Y, and Z are orthogonal coordinates measured along $\bar{a}$, $\bar{b}$, and $\bar{c}^*$ of the unit cell, respectively.

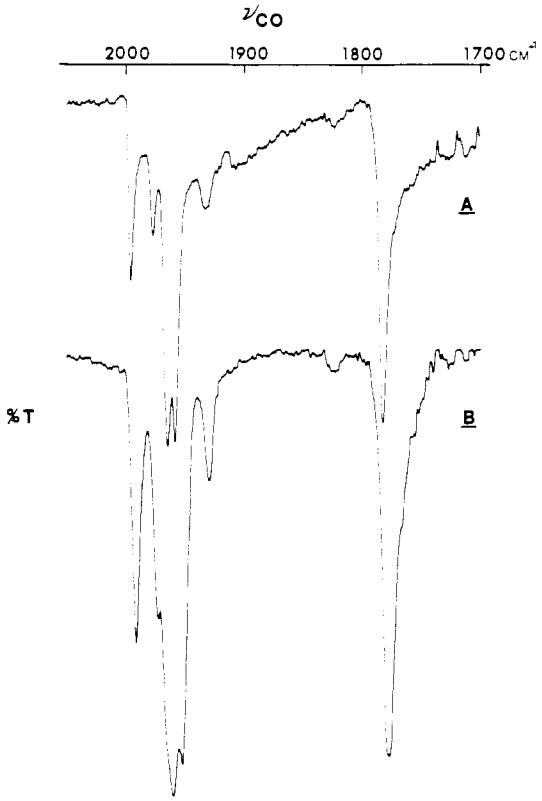

Figure 4. Infrared spectra in ν(CO) region in hexane solution: A, $Ir_4(CO)_8[PMe_3]_4$; B, $Ir_4(CO)_8[PEt_3]_4$.

group between Ir(3) and Ir(4) is tilted out of the basal plane of iridium atoms (see Table V) toward the two axial PMe_3 ligands and away from the apical PMe_3 group. Unfortunately in the related $Ir_4(CO)_9[PPh_3]_3$ molecule, where more dramatic steric effects should exist, the structural parameters were not determined with enough accuracy to assess any differences in metal–metal bond distances.[16] Exclusive of the sterically elongated Ir(3)–Ir(4) bond, the metal–metal bond distances observed in $Ir_4(CO)_8[PMe_3]_4$ are quite similar to those noted in $Ir_4(CO)_{10}$(diars) (apical–basal 2.723–2.731 Å and basal–basal 2.694–2.733 Å), where both arsine donors are bound to a single metal center.[17] In either instance these metal–metal bond distances are slightly longer than the average value determined in parent $Ir_4(CO)_{12}$ species (2.693 Å).[18] The Ir–P bond distances do not vary significantly, ranging from 2.290 (6) to 2.335 (6) Å with an average value of 2.312 Å. These are somewhat shorter than the average Ir–P distance of 2.36 Å reported, for the less basic PPh_3 ligand, in the $Ir_4(CO)_{10}$-

(16) Albano, V.; Bellon, P.; Scatturin, V. *Chem. Commun.* **1967**, 730.
(17) Churchill, M. R.; Hutchinson, J. P. *Inorg. Chem.* **1980**, *19*, 2765.
(18) Churchill, M. R.; Hutchinson, J. P. *Inorg. Chem.* **1978**, *17*, 3528.

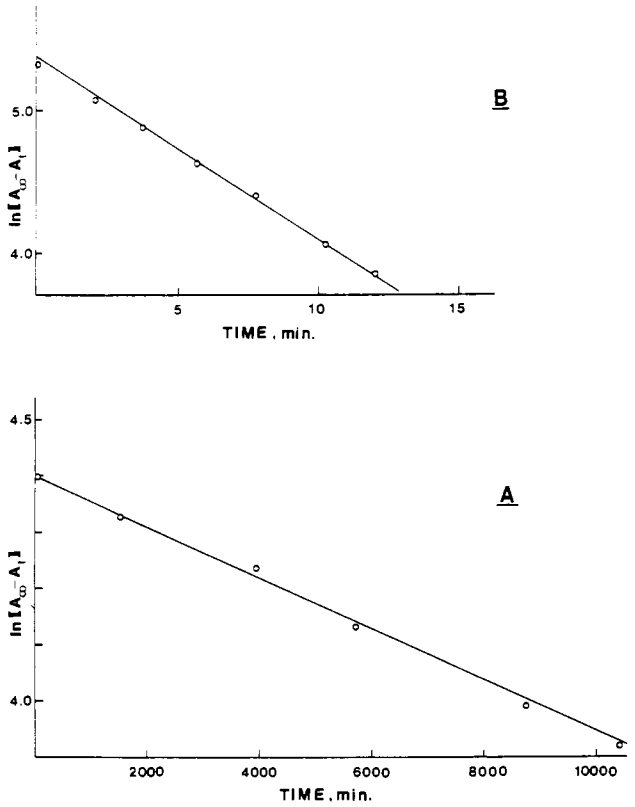

Figure 5. Plot of ln $(A_\infty - A_t)$ vs. time for the substitution of $Ir_4(CO)_8[PR_3]_4$ with CO to afford $Ir_4(CO)_9[PR_3]_3$ at 85.2 °C in tetrachloroethylene: A, R = Me; B, R = Et. Appearance of ν(CO) peak in $Ir_4(CO)_9[PR_3]_3$ was employed in monitoring the reaction.

$[PPh_3]_2$ and $Ir_4(CO)_9[PPh_3]_3$ derivatives.[16]

Stuntz and Shapley[19] have reported ^{31}P and ^{13}C NMR data establishing a solution structure for $Ir_4(CO)_8[PPh_2Me]_4$ which is consistent with that described here for the solid-state geometry of $Ir_4(CO)_8[PMe_3]_4$. In addition, comparative solution infrared investigations in the ν(CO) region, both with respect to the number of vibrational modes and their intensity patterns, of a large variety of phosphine derivatives of the type $Ir_4(CO)_8[PR_3]_4$ indicate all of these species to be isostructural.[20] Figure 4 illustrates typical ν(CO) spectral traces for the $Ir_4(CO)_8[PMe_3]_4$ derivatives where $PR_3 = PMe_3$ and PEt_3.

There is essentially no difference in the basicities of the alkylphosphines Me_3P and Et_3P, where the ΔHNP values are 114 and 111, respectively.[21] On the other hand, we would anticipate significant further crowding around the tetranuclear cluster species upon replacing PMe_3 (cone angle, 118°) in $Ir_4(CO)_8[PR_3]_4$ by PEt_3 (cone angle, 132°).[3] This steric effect is dramatically demonstraed in the relative kinetic lability of the two tetrasubstituted derivatives toward phosphine dissociation as described in eq 3 and 4. These processes were found

$$Ir_4(CO)_8[PMe_3]_4 + CO \xrightarrow{k_1} Ir_4(CO)_9[PMe_3]_3 + PMe_3 \quad (3)$$

$$Ir_4(CO)_8[PEt_3]_4 + CO \xrightarrow{k_2} Ir_4(CO)_9[PEt_3]_3 + PEt_3 \quad (4)$$

to be first order in metal cluster concentration and independent of incoming ligand (CO) concentration (Figure 5). The once formed trisubstituted species were inert toward further phosphine substitution by carbon monoxide. The first-order rate constants, k_1 and k_2, were determined at 85.2 °C in tetrachloroethylene to be 6.35×10^{-7} s^{-1} and 2.09×10^{-3} s^{-1}, respectively. Hence displacement of PEt_3 in $Ir_4(CO)_8[PEt_3]_4$ occurs at a rate which is 3300 times that for the analogous process involving PMe_3.

Because of the great similarity in donor/acceptor ratio[22] of these two trialkylphosphine ligands, it appears safe to ascribe this *substantial* rate enhancement in phosphine displacement from the tetrasubstituted metal cluster species in going from PMe_3 to PEt_3 to steric acceleration. Therefore, this investigation adequately points out the large variation in rates possible for ligand dissociation processes involving metal cluster derivatives which can arise from steric effect alone. Further studies employing a wide range of phosphorus donor ligands are needed, however, before a generalization can be made. These are presently in progress. It is also expected that similar steric arguments can be responsible for large differences in rates of dissociative CO substitutional processes in metal cluster species. Efforts are currently under way in our laboratory to assess steric effects on dissociative processes of carbon monoxide in tetranuclear carbonyl clusters as described in eq 1. Initial results indeed indicate steric considerations to be of paramount importance in these ligand substitutional processes.

Acknowledgment. The financial support of this research by the National Science Foundation (Grant CHE 80-09233) is greatly appreciated.

Registry No. $Ir_4(CO)_8[PMe_3]_4$, 78715-94-3; $Ir_4(CO)_8[PEt_3]_4$, 37366-31-7; $Ir_4(CO)_{12}$, 18827-81-1; CO, 630-08-0.

Supplementary Material Available: A listing of the observed and calculated structure factors (22 pages). Ordering information is given on any current masthead page.

(19) Stuntz, G. F.; Shapley, J. R. *J. Am. Chem. Soc.* **1977**, *99*, 607.
(20) Darensbourg, D. J.; Baldwin-Zuschke, B. J., unpublished results.
(21) Streuli, C. A. *Anal. Chem.* **1960**, *32*, 985.
(22) Bodner, G. M.; May, M. P.; McKinney, L. E. *Inorg. Chem.* **1980**, *19*, 1951.